P2.4

SYNOPTIC RESPONSES TO BREAKING MOUNTAIN GRAVITY WAVES MOMENTUM DEPOSIT AT TURNING CRITICAL LEVELS

Armel MARTIN[1] and François LOTT
Ecole Normale Superieure, Paris, France

1 Abstract

The synoptic scale responses of a stratified rotating shear flow to small scale mountain gravity waves (GWs) encountering turning critical levels is analysed. To quantify the significance of the momentum deposit by the moutain GWs onto the large-scale flow, these responses are compared to those produced by large scale mountains.

For this purpose, we use a semi analytical model based on a linear Boussinesq semi-geostrophic f-plane version of the Eady model of baroclinic instability, and force it by two independent processes. Both processes result from a large scale complex mountain that consists of a finite size ensemble of small scale ridges embedded within a large scale enveloppe, the horizontal scale of the enveloppe being significantly different from that of the individual ridges. Under this hypothesis, a first mountain forcing is due to the mountain GWs which are generated by the small-scale ridges. They interact with the large scale flow at turning critical levels, where they produce a dipolar potential vorticity (PV) anomaly advected and steered by the shear in the mid-troposphere. The second forcing is due to the large scale enveloppe, which produces a vertical velocity at the ground but no inflow PV.

First, we study the model response in the absence of any upper boundary. We show that, under a geometrical configuration such that the majority of the mountain GWs encounter critical levels, the potential vorticity they produce can force steady boundary Eady waves as much substantial as those produced by the corresponding large scale mean orography. Furthermore, we find that the GW can reinforce (i) the anticyclonic circulation and (ii) the downslope low which are produced by the mean orography. We also distinguish between the warm front configurations and the cold front configurations.

In the presence of a rigid lid, baroclinic instabilities can develop but the above results remain valid at least within the first 36 hours. In the long term, the PV advected in the far field can sustain very efficiently the developpment of baroclinic unstable Eady modes.

These calculations are essentially analytical, and illustrate in a well known model the significance of breaking mountain GW and turning critical levels for the synoptic circulation. They may help to appreciate the needs for the parametrization of turning critical levels in GCMs, and in particular the need to parametrize mountain gravity waves in the spectral space. They also give some hints of the benefits to be expected from such parametrizations.

2 Model

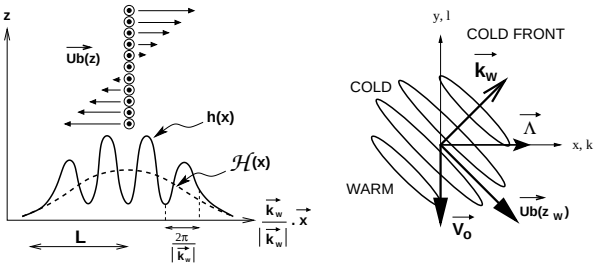

Figure 1: *Diagram of the problem in the cold front situation. The vector* $\mathbf{k_w}$ *defines the transverse scale of the ridges and their orientation.*

We study the synoptic response of a rotating stratified shear flow to the presence of an isolated mountain constituted of several near 2D narrow ridges embedded within a large scale enveloppe of shape $\mathcal{H}(\mathbf{x})$. For this, we take for the mountain elevation (see Fig. 1)

$$h(\mathbf{x}) = H_0\, e^{-\frac{x^2+y^2}{2L^2}} (1+cos(\mathbf{k}_w\mathbf{x})) = \mathcal{H}(\mathbf{x})(1+cos(\mathbf{k}_w\mathbf{x})) \quad (1)$$

where $\mathbf{k}_w = k_w\mathbf{e}_x + l_w\mathbf{e}_y$, and $k_w > 0$ by convention.

The background wind varies linearly with altitude :

$$\mathbf{U}_b(z) = U_b(z)\,\mathbf{e}_x + V_0\,\mathbf{e}_y = (U_0 + \Lambda z)\,\mathbf{e}_x + V_0\,\mathbf{e}_y, \quad (2)$$

[1]Armel MARTIN, Ecole Normale Superieure, Laboratoire de Météorologie Dynamique du CNRS, 24 rue Lhomond, 75235 PARIS cedex 05, France - TEL: -33-01-44322238 - email: martin@lmd.ens.fr

where U_0 and V_0 are the two components of the incident wind at the ground, and Λ is the vertical wind shear. The background potential temperature is assumed to be given by

$$\Theta_b(y,z,t) = \theta_r + \theta_0(z) + \Theta(y) + \theta_{ad}(t), \qquad (3)$$

where θ_r is a constant reference temperature, $\theta_0(z)$ is the stratification when the fluid is at rest,

$$\Theta(y) = -\frac{\Lambda f \theta_r}{g}\, y \qquad (4)$$

equilibrates the shear via the thermal wind balance, and

$$\theta_{ad}(t) = -V_0 \Theta_y\, t \qquad (5)$$

accounts for the global change of potential temperature associated to the front Θ_y advancing at the velocity V_0. The indices y and z denote derivatives relative to the corresponding coordinate. The gradients of $\theta_0(z)$ and $\Theta(y)$ are both constant, which implies that the Brunt Väisälä frequency and the background wind shear,

$$N^2 = \frac{g\theta_{0z}}{\theta_r} \quad \text{and} \quad \Lambda = -\frac{g\Theta_y}{f\theta_r}, \qquad (6)$$

are constant too.

Next, we assume that the response to the large scale enveloppe $\mathcal{H}$ is well described by balanced equations, while the response to the small scale orography $\mathcal{H}(\mathbf{x})\, cos(\mathbf{k}_w\, \mathbf{x})$ is well described by GWs not sensitive to the Coriolis force. These hypotheses at least require that the characteristic scale of the enveloppe is large compared to that of the GWs ($\|\mathbf{k}_w\| L \gg 1$), and that the Rossby number associated with the GWs is large ($\frac{V_0}{f}\, \|\mathbf{k}_w\| \gg 1$). Nevertheless, if the background flow turns with altitude, the GWs can encounter critical levels (Shutts, 1998), and affect the large scale flow as they deposit momentum and produces PV anomalies (Schär and Smith, 1993). The large scale flow response to this process will also be analysed with the balanced equations used to describe the response to $\mathcal{H}$. Therefore, in the rest of the paper, we will assume that the large scale flow only sees the GWs through a large scale force

$$\mathbf{F}(\mathbf{x},z) = F(\mathbf{x},z)\, \mathbf{e}_x + G(\mathbf{x},z)\, \mathbf{e}_y, \qquad (7)$$

and assume that the horizontal scale of this force is comparable to that of $\mathcal{H}$, and that this scale corresponds to a Rossby number near 1 or smaller. Under this last hypothesis, and for small amplitude forcings, the response to $\mathbf{F}$ and $\mathcal{H}$ can be evaluated analitycally using a linear version of the semi-geostrophic Boussinesq set of equations given in Hoskins (1975). Indeed, Lott (2003) has shown that semi-geostrophic equations describe very well the large scale response to breaking GWs in complete numerical simulations.

This set of equations satisfies a budget for the potential vorticity (PV) given by :

$$(\partial_t + \mathbf{U}_b \nabla)\, q + \nabla \mathbf{J}_N = 0, \qquad (8)$$

where the non advective PV flux and the PV are respectively

$$\mathbf{J}_N = -\,\theta_{0z}\,(1 - Ri^{-1})\,\mathcal{G}\,\mathbf{e}_x + \theta_{0z}\,\mathcal{F}\,\mathbf{e}_y - \Theta_y\,\mathcal{F}\,\mathbf{e}_z \quad (9)$$

and

$$q(\mathbf{x},z,t) = \theta_{0z}\left((1 - Ri^{-1})\partial_x v_g - \partial_y u_g\right) + \Theta_y \partial_z u_g + f\partial_z \theta. \qquad (10)$$

In Eqs. (9) and (10), $R_i = \frac{N^2}{\Lambda^2}$ is the background flow Richardson number. This linear problem can be solved in the Fourier space in the horizontal directions. In this space, the PV can be evaluated analytically and the potential satisfies :

$$\frac{\partial^2 \hat{\phi}}{\partial z^2} - 2i\lambda_i \frac{\partial \hat{\phi}}{\partial z} - \left(\lambda_r^2 + \lambda_i^2\right)\hat{\phi} = \frac{g}{f\theta_r}\hat{q}, \qquad (11)$$

$$\text{where } \lambda_r = \frac{N}{f}\sqrt{1 - \frac{1}{Ri}}\|\mathbf{k}\| \text{ and } \lambda_i = l\frac{\Lambda}{f}. \qquad (12)$$

Therefore, the general form of the potential is :

$$\hat{\phi} = \hat{\phi}_p(\mathbf{k},z,t) + \hat{\phi}_u(\mathbf{k},t)\, e^{-\lambda z} + \hat{\phi}_d(\mathbf{k},t)\, e^{+\lambda^*(z-D)}, \qquad (13)$$

where the particular solution

$$\hat{\phi}_p(\mathbf{k},z,t) = e^{-\lambda z}\int_0^z e^{2\lambda_r z'}\int_{z'}^D -\frac{g}{f\theta_r}\hat{q}\, e^{-\lambda^* z"}\, dz"\, dz' \qquad (14)$$

($\lambda = \lambda_r - i\lambda_i$) contains all the PV, but vanishes in $z = 0$ and $z = D$ ($*$ denotes the complex conjuguate). The two other terms are the eigenmodes of Eq. (11) with a null right hand, which contain no PV, but which satisfy the two boundary conditions (boundary Eady waves).

We split each boundary Eady mode and each boundary condition in two parts :

$$\hat{\phi}_{u,d}(\mathbf{k},t) = \hat{\phi}_{u,d_W}(\mathbf{k},t) + \hat{\phi}_{u,d_E}(\mathbf{k},t), \qquad (15)$$

where the indices W and E respectively refer to the part excited by the GWs, and the part excited by the large scale enveloppe. The temporal evolution is obtained by the four boundary conditions. At the ground :

$$\lambda_r(\partial_t - i\mathbf{k}\mathbf{U_0})\left(\hat{\phi}_{u_W} - \hat{\phi}_{d_W}\, e^{-\lambda^* D}\right)$$

$$-ik\Lambda\left(\hat{\phi}_{u_W} + \hat{\phi}_{d_W}\, e^{-\lambda^* D}\right) = B_G(\mathbf{k},t)\ \text{, with} \qquad (16)$$

$$B_G(\mathbf{k},t) = (\partial_t - i\mathbf{k}\mathbf{U_0})\,\partial_z\hat{\phi}_p(0) + \Lambda\hat{F}(0)\ \text{, and} \qquad (17)$$

$$\partial_z\hat{\phi}_p(0) = -\int_0^D \frac{g}{f\theta_r}\,\hat{q}\, e^{-\lambda^* z} dz = \partial_z\hat{\phi}_p(\mathbf{k}, z=0, t)\ , \qquad (18)$$

and second

$$\lambda_r(\partial_t - i\mathbf{k}\mathbf{U_0})\left(\hat{\phi}_{u_E} - \hat{\phi}_{d_E}\, e^{-\lambda^* D}\right)$$

$$-ik\Lambda\left(\hat{\phi}_{u_E}+\hat{\phi}_{d_E}\,e^{-\lambda^* D}\right)=-i\mathbf{k}\mathbf{U_0}\,N^2\left(1-\frac{1}{Ri}\right)\hat{\mathcal{H}}(\mathbf{k}), \tag{19}$$

where $\hat{F}(0)=\hat{F}(\mathbf{k},z=0)$. At the tropopause we impose to the vertical velocity to vanish (the equations are not shown but very near Eqs. (16)-(19)). We always take a null initial state, and the balanced response is always described at the ground, where $\hat{\phi}_p$ vanishes, therefore we are only interested in comparing the two Eady modes :

$$\hat{\phi}_W(\mathbf{k},t)=\hat{\phi}_{u_W}(\mathbf{k},t)+\hat{\phi}_{d_W}(\mathbf{k},t)\,e^{-\lambda^* D} \text{ and}$$

$$\hat{\phi}_E(\mathbf{k},t)=\hat{\phi}_{u_E}(\mathbf{k},t)+\hat{\phi}_{d_E}(\mathbf{k},t)\,e^{-\lambda^* D}. \tag{20}$$

To evaluate the force $\mathbf{F}(\mathbf{x},z)$, we make another hypothesis and assume that its horizontal repartition takes the form :

$$\mathbf{F}(\mathbf{x},z)=\overline{\mathbf{F}}(z)\,e^{-\frac{x^2+y^2}{L^2}}\text{, where } \overline{\mathbf{F}}=-\frac{d}{dz}\overline{\mathbf{u}\,w}\text{, and} \tag{21}$$

$$\overline{\mathbf{u}w}=\frac{1}{\pi L^2}\int_{-\infty}^{+\infty}\int_{-\infty}^{+\infty}\mathbf{u}\,w\,dx\,dy \tag{22}$$

Under this hypothesis, we can calculate analytically $\overline{\mathbf{F}}$. As the most of the GWs emitted by the mountain have $\mathbf{k}$ that is near $\mathbf{k}_w$ (or $-\mathbf{k}_w$), the forcing $\mathbf{F}$ is only significant if there exists an altitude z_w where the background wind is perpendicular to $\mathbf{k}_w$, i.e. the background wind has to pass from one side of the ridges to the other when z increases. Such a favorable configuration is shown in the Fig. 1, and in this case we obtain

$$\overline{\mathbf{F}}(z)\approx F_0\,\frac{U_b(z)}{\|\mathbf{U}_b(z)\|^2}\,k_0(z)^2\,e^{-L^2\|\mathbf{k}_w\|^2+L'^2k_0^2}$$

$$(V_0\,\mathbf{e}_x-U_b(z)\,\mathbf{e}_y)\,, \tag{23}$$

$$F_0=\frac{1}{2\sqrt{\pi}}\,H_0^2\,L\,N\,\Lambda\,, \tag{24}$$

$$k_0=\frac{k_w-l_w\frac{U_b(z)}{V_0}}{1+\frac{U_b(z)^2}{V_0^2}}\;;\;L'^2=\left(1+\frac{U_b(z)^2}{V_0^2}\right)L^2. \tag{25}$$

The vertical profile of $\overline{\mathbf{F}}$ in Eq. (23) is displayed in Fig. 2, for the cold front configuration presented in Fig. 1 (parameters given in section 3). It is noteworthy that whatever is the altitude z, $\overline{\mathbf{F}}(z)$ is perpendicular to the background wind $\mathbf{U}_b(z)$, which is a characteristic feature of breaking GWs at critical levels. The force reaches its maximum at $z_w=5km$, which is the altitude of the critical level associated to $\mathbf{k}_w$, the wave vector for which the spectrum of GWs is maximum. The force is significant over a vertical width of about 1-2km, centered around z_w, which will refer to the critical zone in the rest of the paper.

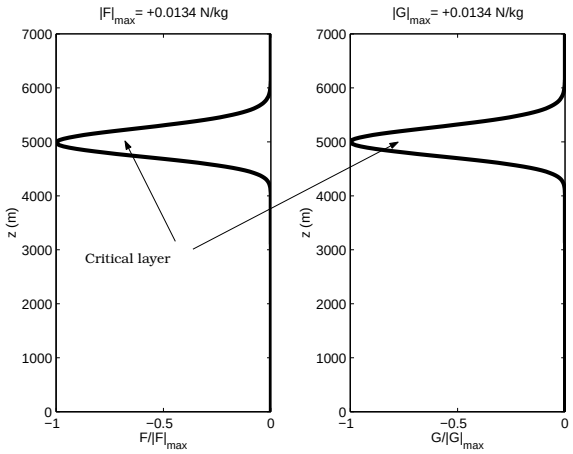

Figure 2: *Vertical profile of the forcing $\overline{\mathbf{F}}(z)$, calculated in the reference cold front configuration described in section 3.*

Numerical resolution:

To determine the flow response, we first integrate $\hat{\phi}_p$ using Eq. (14), by a trapezoïdal method on a model with a vertical grid which resolution is 500 m. Then, $\hat{\phi}_W$ and $\hat{\phi}_E$ are computed from the first order differential Eq. (16),(19), and the two upper boundary conditions, in the horizontal Fourier space and for $512*512$ harmonics. The corresponding horizontal mesh size in the physical space is $40\,km*40km*500\,m$, for a $10000\,km*10000\,km*10\,km$ global domain box. The temporal integrals are computed with a trapezoïdal method too, and the model's time step is $DT=6H$.

3 Results

We first present the response for the idealized cold front situation in Fig. 1. The parameters are chosen as follows :

$$f=10^{-4}\,s^{-1}\;,\;N=10^{-2}\,s^{-1}\;,\;\Lambda=4.10^{-3}\,s^{-1}$$

$$U_0=0 \text{ and } V_0=-20\,ms^{-1}$$

The parameters that define the orography are :

$$H_0=800 \text{ m }, L=200 \text{ km, and } |\mathbf{k}_W|=\frac{2\pi}{70000}\,m^{-1}.$$

These values lead to a dimensionless mountain height $\epsilon=\frac{NH_0}{V_0}\approx 0.4<1$, for the mean orography and $\epsilon=\frac{N\,2H_0}{V_0}<0.8<1$ for the small scale orography, which justifies a linear treatment. The large scale Rossby number is then $\frac{V_0}{f\,L}\sim 1$. We also take $\widehat{(\mathbf{e}_x;\mathbf{k}_w)}=\frac{\pi}{4}$, so that the critical zone centers around the altitude z_w such that :

$$\mathbf{k}_w.\mathbf{U}_b(z_w)=0 \text{ that is } z_w=5\,km. \tag{26}$$

In the following, we will refer to that case as the Reference Cold Front Configuration (RCFC).

3.1 Potential vorticity anomaly

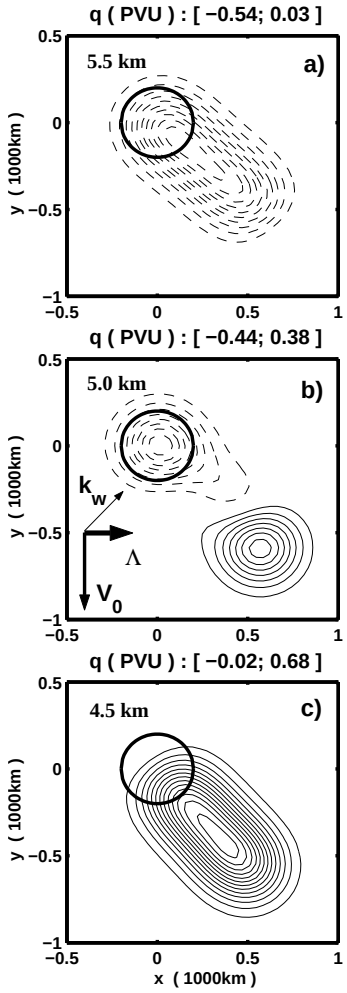

Figure 3: *Potential vorticity anomaly at $t = 8h$, in the reference cold front configuration (RCFC) (CI=0.05 PVU, 1 PVU=$1.0 * 10^{-6}\, K\, kg^{-1}\, m^2\, s^{-1}$). Horizontal sections are shown in the critical zone, centered at $z_w = 5km$. The range of values obtained is indicated above each section and the negative contours are dashed. The mountain is symbolized by the thick circle.*

The Fig. 3a,b and c show three horizontal sections of the PV anomaly due to $\mathbf{F}$ (Eqs. (8)-(10)), expressed in PV units (1 PVU=$1.0 * 10^{-6}\, K\, kg^{-1}\, m^2\, s^{-1}$). At the three altitudes, the PV pattern is predominantly oriented in the direction of the background wind $\mathbf{U}_b(z_w)$. This general orientation follows that, once produced by the non-advective PV flux $\mathbf{J}_N$ that is maximum near the point $(\mathbf{x} = \mathbf{0}; z = z_w)$ (Fig. 3b), the PV anomaly is advected by the background flow.

Furthermore, it is noteworthy that the sign of the PV changes vertically. This follows that the non advective PV flux $\mathbf{J}_N$ has a vertical component $-\Theta_y F$ proportionnal to V_0, hence oriented downward in this cold front case (Fig. 3a), and with a maximum value at $z = z_w$ (Fig. 3b). Because of this vertical asymmetry of the PV anomaly, with the positive lobe under the critical layer and the negative one above, one can expect its influence near the ground to be predominantly cyclonic.

It may be emphasized here that the pattern, presented in Figs.3b, is strongly reminiscent of what occurs for a start-up cyclone in a barotropic flow over large scale mountains (Fig. 4). Lott (1999) has shown that such a start-up cyclone and the associated anticyclone attached to the ridge, are the natural consequence of a force acting perpendicularly to the flow, as it is the case here.

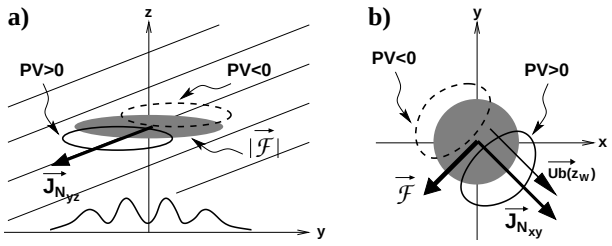

Figure 4: *Schematic representation of the mechanism that produces the 3D PV disturbance in the model for the RCFC, in the vicinity of the mountain, where the non advective part of the PV flux $\mathbf{J_N}$ is dominant. a) Section at $x = 0$; b) Section at $z = z_w$. The schematic contours of PV correspond to values found near the start up $t = 0$.*

3.2 Surface Potential

The time evolution of the surface potential ϕ_E, due to $\mathcal{H}$, is shown in fig. 5 a,b and c every 12 hours.

Consistent with Smith (1986), a stable boundary Eady wave is developping and extending downwind. This baroclinic lee wave is characterized by an anticyclonic pattern standing on the mountain. Immediately downstream of the mountain a trough is taking place, whose minimum reaches -1.3 mbar after 36 hrs (Fig. 5c).

The evolution of ϕ_W, the surface potential due to $\mathbf{F}$, is shown in fig. 5 d, e and f. As expected, the breaking GWs also excite a boundary Eady wave, with a minimum magnitude comparable to that of ϕ_E. At t=36hrs, the minimum and maximum reach respectively -1.1 mb and 0.7 mb. Nevertheless, several differences are noticeable : i) the GWs do not induce a persistant anticyclonic pattern over the mountain; ii) the main cyclonic lobe is developping along the axis of the background wind in the critical zone, that is at -45° of the x-axis; iii) the wavelength of the disturbance is about 2000 km, and substantially larger than that of ϕ_E.

Recalling that the PV anomaly q, in our system, is felt at the ground through the weighted average in Eq. (18), we can explain these three differences : i) follows that the positive PV lobe at $z = 4.5\,km$ hides in part the predominantly negative PV values found over the mountain and above that altitude (Fig. 3.a and 3.b); ii) follows that the PV anomaly extends along the -45° direction as well (Fig. 3); and iii) follows that the e-folding vertical decay length $\frac{1}{\lambda_r}$ in Eq. (18) decreases when the horizontal wavenumber increases.

The fig. 5 g,h and i show the sum of the two contributions. The extrema observed at t=36 hrs show that the first downstream trough induced by the enveloppe (ϕ_E) is slightly reïnforced by the GWs and reaches -1.6 mb, while the anticyclone over the mountain is almost unchanged. Notably, the trough just in the lee of the mountain, that is in the first thousand of kilometers, is slightly deepened.

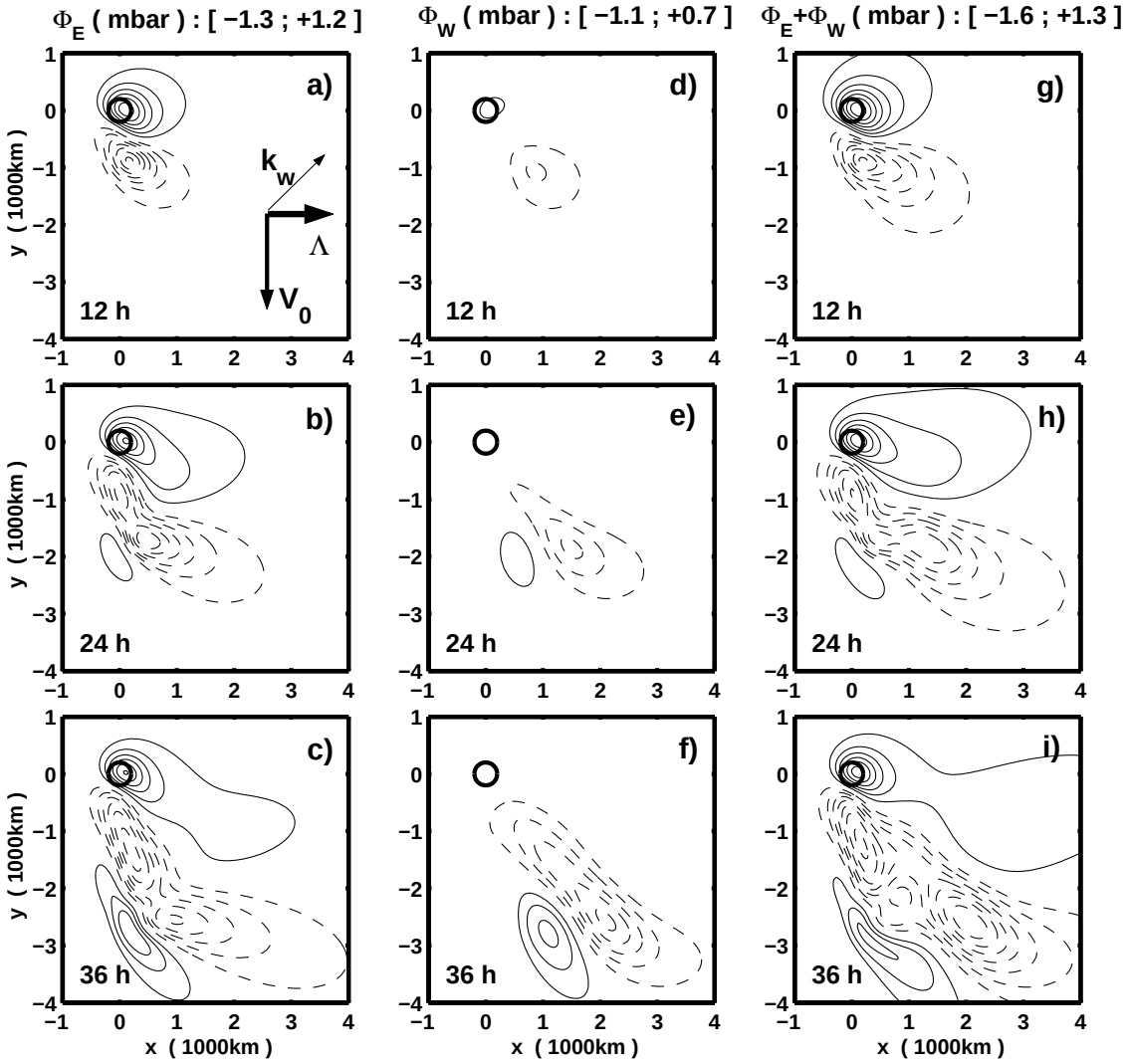

Figure 5: *Evolution of the potential at the surface in the RCFC, with the same conventions as in fig. 3 (CI=0.2 mbar). a), b) and c) : part of the potential excited by the enveloppe of the mountain $\mathcal{H}(\mathbf{x})$ (ϕ_E), respectively at t=12 hrs, 24 hrs and 36 hrs; d), e) and f) : part of the potential due to the inflow PV anomaly deposited by the breaking GWs (ϕ_W); g), h) and i) : total disturbance at the surface ($\phi_E + \phi_W$). The extreme values reached at t=36 hrs are indicated at the top of each column.*

4 Sensitivity tests

The warm front configuration

A Reference Warm Front Configuration (RWFC) is specified by inverting the wind at the surface :

$$V_0 = 20\ ms^{-1}$$

To obtain a significant force $\mathbf{F}$ in that case we also need to rotate the ridges and take $l_w = -k_w < 0$. All the other parameters stay equal to those in the previous case.

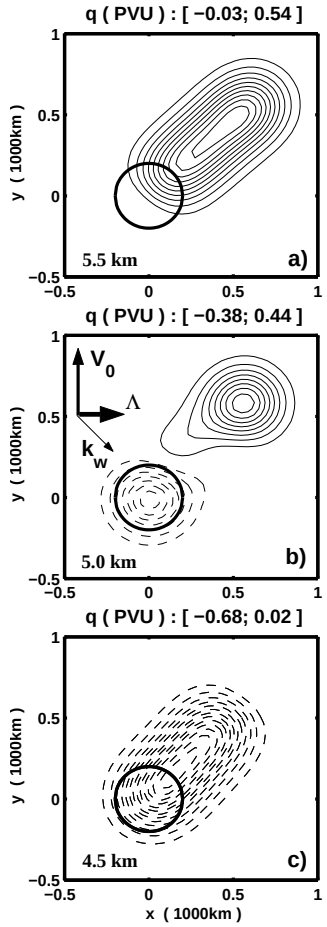

Figure 6: *Potential vorticity anomaly at $t = 8h$, in the RWFC, with the same conventions as in fig. 3 (CI=0.05 PVU).*

The PV anomaly obtained has the same dipolar struture as in the RCFC, it is oriented along the background wind near z_w, which is south-west north east (Fig. 6). Because of this asymmetry, and while the response to the enveloppe ϕ_E is exactly the mirror image as regards to the x-axis of that found in the cold front case (Fig. 7a, b and c), the response to the breaking GWs ϕ_W is not symmetrical to the previous one (Fig. 7d, e and f). More precisely, now the boundary Eady wave is dominated by a strong anticyclonic lobe which stays attached to the mountain. Notably, in this RWFC, the breaking mountain GWs reïnforce both the downslope trough and the anticyclone over the mountain.

Results with a tropopause : allowing baroclinic instability

Now we come back to the initial problem of section 2, and we consider the existence of an upper rigid lid at the altitude $D = 10\,km$, allowing baroclinic instability. We find that under approximately one day and a half, the baroclinic growth is negligeable, which justifies the previous approach without any upper boundary. Thereafter, a substantial signal due to unstable modes start to dominate the response in the far field (i.e. far from the mountain range, and attached to the PV anomalies produced in the first few hours and that are advected downstream).

5 Conclusion

In this paper we have presented the building up and the use of a rather simple tool for studying the impact of mountain GWs breaking at turning critical levels on the large scale flow. The rather academic and analytical nature of the model allows us to understand the physical mechanisms induced in this problem. An interest of the method is to separate the effect of the large scale mean orography from the effect of the small scale breaking GWs, and to compare their relative importance.

We have shown that the impact of the breaking GWs emitted by the small scales of the orography, in terms of surface potential, can be comparable to the impact of the enveloppe. We have identified the different processes that have an influence on the strength of this effect, and on the characteristics of the pattern at the surface. The relative configuration of the background wind as regards to the vector $\mathbf{k}_w$ defining the orientation and the width of the parallel ridges is crucial. It controls notably the altitude of the critical zone, and thus influences strongly the amplitude of the perturbation at the ground. Typically, a favorable case is obtained when the background wind passes from one side of the ridges to the other when z increases. Furthermore, we have identified some configurations, with a cold front and then a warm front, where the breaking GWs reïnforce both the downslope trough and the anticyclone over the mountain due to the enveloppe. The presence of unstable Eady modes, introduced here by taking into account a rigid lid, does not modify substantially those results, at least during one day or two. In a longer term and in the far field, nevertheless, we also found that GWs can trigger substantial baroclinic instability growth.

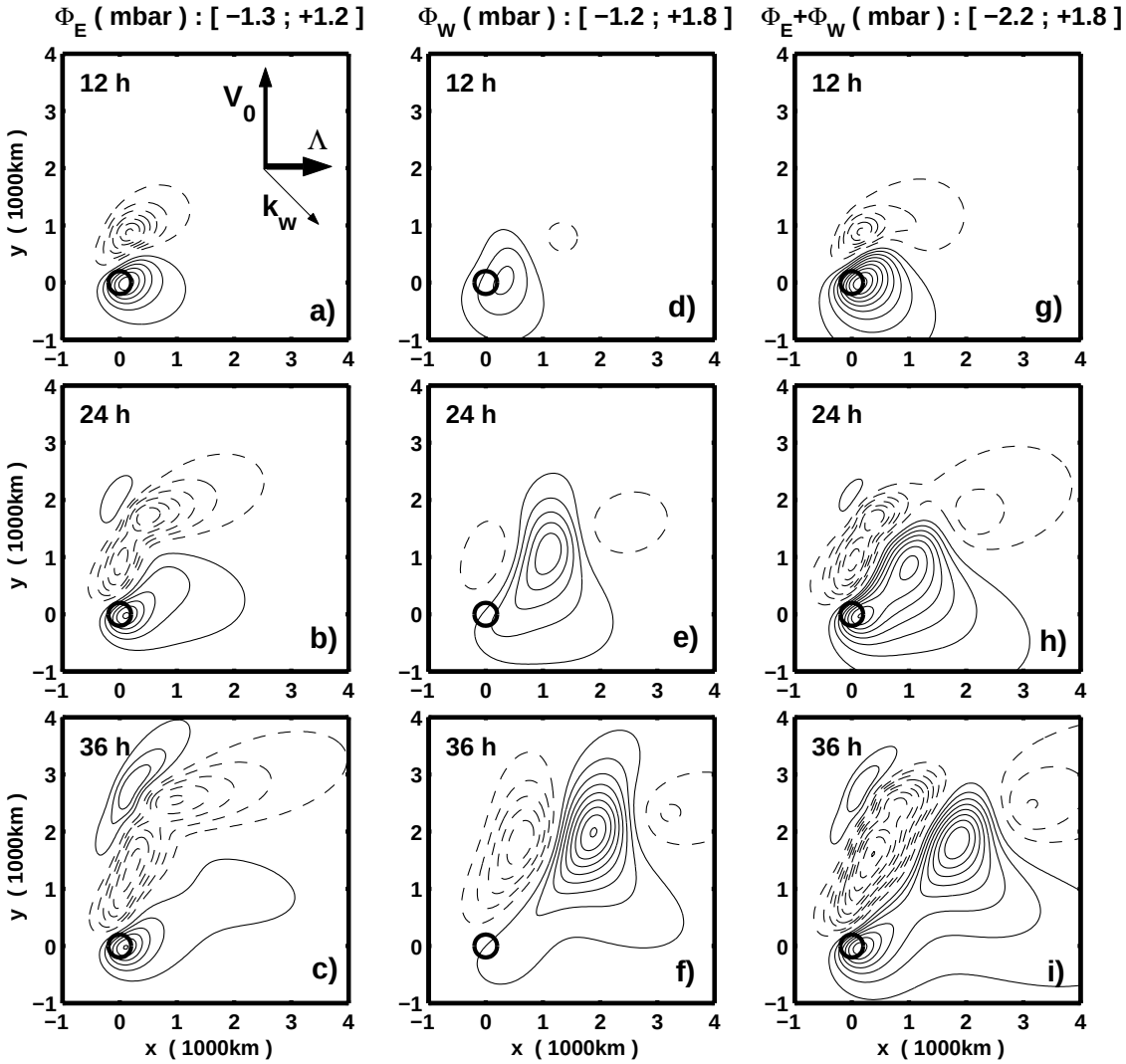

Figure 7: *Evolution of the potential at the surface in the RWFC, with the same conventions as in fig. 5 (CI=0.2 mbar).*

References

[1] Smith R. B. Further development of a theory of lee cyclogenesis. *Journal of the Atmospheric Sciences*, 43(15):1582–1602, August 1986.

[2] Schär C. and Smith R. B. Shallow-water flow past isolated topography. part i: Vorticity production and wake formation. *Journal of the Atmospheric Sciences*, 50(10):1373–1400, May 1993.

[3] Schär C. and Durran D. R. Vortex formation and vortex shedding in continuously stratified flows past isolated topography. *Journal of the Atmospheric Sciences*, 54(4):533–554, February 1997.

[4] Lott F. Alleviation of stationary biases in a gcm through a mountain drag parametrization scheme and a simple representation of mountain lift forces. *Monthly Weather Review*, 127:788–801, 1999.

[5] Lott F. Large scale flow response to short gravity waves breaking in a rotating shear flow. *Journal of the Atmospheric Sciences*, 60:1691–1704, 2003.

[6] Hoskins B. J. The geostrophic momentum approximation and the semi-geostrophic equations. *Journal of the Atmospheric Sciences*, 32(2):233–242, February 1975.

[7] Shutts G. J. Stationary gravity-wave structure in flows with directional wind shear. *Quaterly Journal of the Royal Meteorological Society*, 124:1421–1442, 1998.